

Finite element model for the long-term behaviour of composite steel-concrete push tests

O. Mirza and B. Uy*

School of Engineering, University of Western Sydney, Locked Bag 1797 Penrith South DC, NSW 1797, Australia

(Received December 10, 2007, Accepted November 25, 2009)

Abstract. Composite steel-concrete structures are employed extensively in modern high rise buildings and bridges. This concept has achieved wide spread acceptance because it guarantees economic benefits attributable to reduced construction time and large improvements in stiffness. Even though the combination of steel and concrete enhances the strength and stiffness of composite beams, the time-dependent behaviour of concrete may weaken the strength of the shear connection. When the concrete loses its strength, it will transfer its stresses to the structural steel through the shear studs. This behaviour will reduce the strength of the composite member. This paper presents the development of an accurate finite element model using ABAQUS to study the behaviour of shear connectors in push tests incorporating the time-dependent behaviour of concrete. The structure is modelled using three-dimensional solid elements for the structural steel beam, shear connectors, concrete slab and profiled steel sheeting. Adequate care is taken in the modelling of the concrete behaviour when creep is taken into account owing to the change in the elastic modulus with respect to time. The finite element analyses indicated that the slip ductility, the strength and the stiffness of the composite member were all reduced with respect to time. The results of this paper will prove useful in the modelling of the overall composite beam behaviour. Further experiments to validate the models presented herein will be conducted and reported at a later stage.

Keywords: composite steel-concrete beams; creep; shrinkage; finite element analysis; long term behaviour.

1. Introduction

For composite steel concrete structures, concrete not only provides the compressive strength but also the fire resistance to the floor surface whilst the steel predominantly provides the tensile strength. Johnson (1974) stated that when acting compositely through a shear stud, the composite steel-concrete member is stiffer and stronger. When concrete creep is considered, the deformation will increase with time. Gilbert and Bradford (1995) stated that the time-dependent deformation of concrete due to creep and shrinkage is very complicated and only limited research has been published on the time varying behaviour for composite steel-concrete beams. Composite steel-concrete beam designs are mainly affected by the behaviour of the shear connection. When the creep and shrinkage behaviour of the concrete is considered, the factors affecting the shear connection are the stiffness and strength of shear connectors and the stiffness and strength of the surrounding concrete. The strength of concrete is

*Professor and Head, Corresponding Author, E-mail: b.uy@uws.edu.au

reduced according to time due to creep and shrinkage. Initially, experimental push tests undertaken by Lam and El-Lobody (2005) without the consideration of time dependent effects were used to evaluate the load-slip relationship of the connector using the finite element software package, ABAQUS. The main reason is to prove that the finite element models were accurately developed. Then, the finite element model was incorporated with the creep and shrinkage behaviour. The main objectives of this paper are to develop a three dimensional finite element model which simulates the shear connector behaviour for both solid and profiled slabs where time effects are incorporated for the concrete slab.

2. Time effects of composite steel-concrete structures

Although time dependent deformations for concrete are not a major concern with respect to the collapse of structures, they are important issues that need consideration for serviceability and durability of structures. There are physically two different types of time dependent deformations for concrete. One is purely dependent on the stress which is known as the creep strain, ε_{cr} and the other is independent of stress and is known as the shrinkage strain, ε_{sh} .

Even though creep of concrete is considered to cause deformations with increasing time, there is no evidence of significant damage to concrete material. Concrete structures whose long-term serviceability has been compromised by creep deformation resulting in a drastic reduction of their design life include studies by Bazant and Tsubaki (1980) and Mazzotti and Savoia (2003).

Creep significantly affects the structural behaviour at service loads. Creep causes the strain of concrete gradually to increase with time under sustained stress. Compared with instantaneous deformations, the deformations of a member associated with time and may reach a value which is several times greater than the instantaneous deformation. Gradual development of creep increases the curvature and thus results in increased beam deflections. The age of concrete at the instant of loading is very influential in creep. Furthermore, creep also is highly dependant on humidity, temperature and the area which is exposed to the environment.

A typical stress-strain curve for concrete is shown in Fig. 1. Under service load conditions, a linear relationship is assumed. The instantaneous strain $\varepsilon_c(t_0)$ that occurs immediately after the stress application $\sigma_c(t_0)$ at time t_0 can be described in Eq. (1)

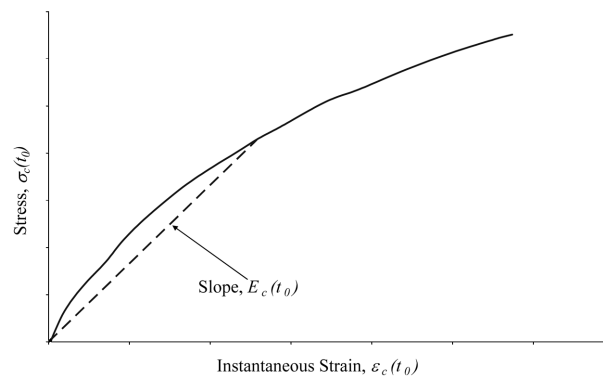


Fig. 1 Stress-strain relationship for concrete

$$\varepsilon_c(t_0) = \frac{\sigma_c(t_0)}{E_c(t_0)} \tag{1}$$

where t_0 = time of application of the stress
 $\sigma_c(t_0)$ = applied concrete compressive stress
 $E_c(t_0)$ = modulus of elasticity of concrete at age t_0

When a sustained stress is applied a time t , the strain due to creep with increasing time is defined in Eq. (2) and Fig. 2 can be plotted using this equation.

$$\varepsilon_{cr}(t) = \frac{\sigma_c(t_0)}{E_c(t_0)} [1 + \varphi(t, t_0)] \tag{2}$$

From Fig. 2, the creep coefficient can be defined as the ratio of creep strain to instantaneous strain where this value depends heavily on the age of concrete when the stress is first introduced. The value increases according to the age of concrete but reduces at a descending rate and ceases after 2 to 5 years. Depending on the concrete strength, the final strain value is about 1.2 to 3 times the magnitude of the instantaneous strain.

Due to the limited experimental data available regarding the strength of concrete due to creep, a simple model from CEB-FIP (1990) is used for the creep damage strength interaction of concrete. The stress and strain law is used to describe the concrete behaviour as a function of its strength. The different ageing time of stress and strain law of concrete is given in Fig. 3.

From Fig. 3, the concrete with stiffness and strength evaluated at:

- time at t_0 where
 $\varepsilon^{el,d}(t_0)$ = the effective strain which is the sum of instantaneous strains
 $\varepsilon_{eff}^v(t_0, \delta t) = \beta$ is a fraction of viscous strain which is obtained from an age of loading at time t_0
 Δt is a time under loading which is $t_r - t_0$
- time at t_r where
 $\varepsilon^{el,d}(t_r)$ = is the effective strain which is the sum of instantaneous strain

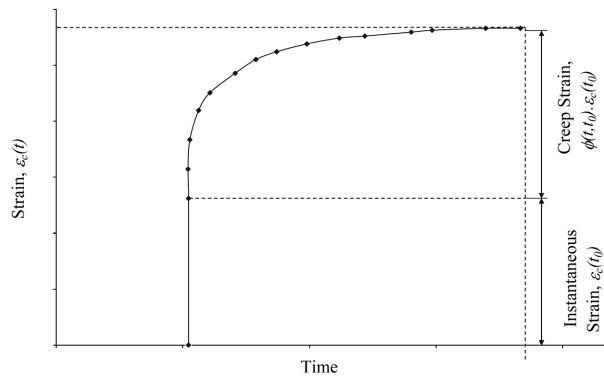


Fig. 2 Creep under sustained stress, Ghali, *et al.* (2002)

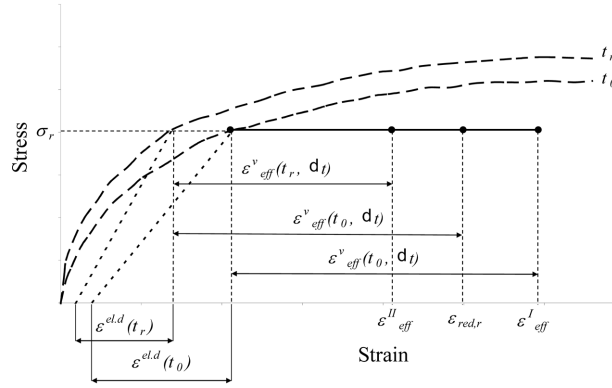


Fig. 3 Stress and strain relationship of concrete with respect to time, CEB-FIP (1990)

$\epsilon_{eff}^v(t_r, \delta t) = \beta$ is a fraction of viscous strain which is obtained from an age of loading at time t_r , Δt is a time under loading

Where $\epsilon^{el,d}(t_0) > \epsilon^{el,d}(t_r)$ and $\epsilon_{eff}^v(t_0, \Delta t) > \epsilon_{eff}^v(t_r, \Delta t)$ to produce $\epsilon_{eff}^I > \epsilon_{eff}^{II}$

When creep is considered, the Poisson's ratio also changes according to time. Various proposals have been presented by Krajcinovic and Fonseka (1981) and di Prisco and Mazars (1996) to define the Poisson ratio evolution as a function of longitudinal strain. Models that best fit experimental results were developed by Kupfer, *et al.* (1969) and Mazzotti, *et al.* (2000) which are known respectively as regression models and power law as is shown in Fig. 4.

When the composite steel-concrete structure is exposed to a dry atmosphere, the concrete element will gradually shrink. The rate of shrinkage strain is gradually increased with time at a reduced rate shown in Fig. 5.

According to CEB-FIP (1990), the development of shrinkage starts at time t_s , when moist curing stops and strain starts to develop for a time $t > t_s$ and is defined in Eq. (3) below:

$$\epsilon_{cs}(t, t_s) = \epsilon_{cs0} \beta_s (t - t_s) \tag{3}$$

where ϵ_{cs0} is the notation given to the shrinkage coefficient. The value depends upon the quality of

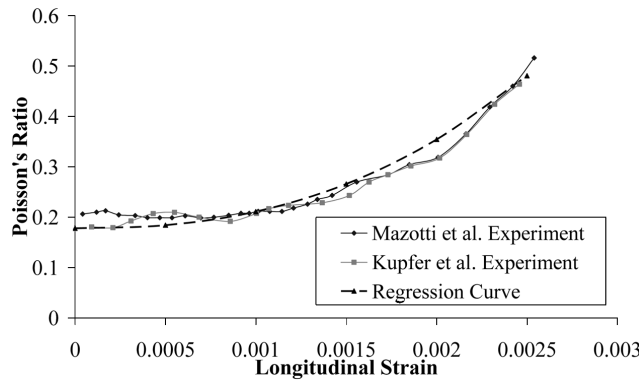


Fig. 4 Poisson's ratio versus longitudinal strain for concrete, Mazzotti and Savoia (2003)

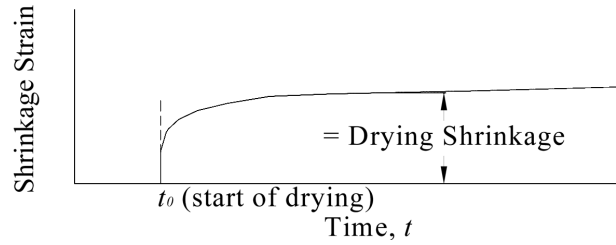


Fig. 5 Shrinkage curve with respect to time, Bazant and Jirasek (2002)

concrete and the environments humidity.

β_s is the coefficient to represent the development of shrinkage according to time

t is the age of concrete in days

t_s is the age of concrete in days when shrinkage starts

Time dependent analysis for composite steel and concrete beams with shear connectors including slip between the steel and concrete interface from Tarantino and Dezi (1992) proved that the stresses in the concrete depend on the stiffness of the connection system. In contrast, Bradford (1991) affirmed that due to creep and shrinkage, the shear force per unit length of connectors tends to decrease with time and most importantly, the stiffness connectors have less influence on deflection.

Bradford and Gilbert (1989, 1992) used a simplified approach to evaluate creep and shrinkage effects in steel concrete composite beams based on the age-adjusted effective modulus to model the stress and strain relationship for concrete where the aging coefficient, χ was introduced and verified that residual stress resulted in decreased concrete stiffness. Moreover, it also demonstrated that the effect of creep and shrinkage dominated the reduction in concrete stiffness at service loads. The authors were supported by an analytical model with a layer approach undertaken by Kwak, *et al.* (2000).

Tarantino and Dezi (1992), Dezi, *et al.* (1995) and Dezi and Tarantino (1993) studied the creep analysis of composite beams where the flexibility of shear connection was taken into account. These studies are to investigate the effect of slip on the steel-concrete interface and determine the distribution of the shear force of the composite steel-concrete beams.

Dezi, *et al.* (1998) simplified the complex numerical methods with a method known as the algebraic method. The algebraic method is a method used for non-complex composite structures. However, for shear connectors, the authors used the pseudo-elastic analysis because the headed stud shear connectors are known to behave in a complex manner. This study is made possible by defining a modified Young's Modulus for concrete. These methods are the effective modulus method, EM and the mean stress method, MS. The creep effect is evaluated by means of a pseudo-elastic analysis using the EM method and is defined in Eq. (4) whilst the shrinkage effect is modified by creep and is evaluated by means of a pseudo-elastic analysis using the MS method as defined in Eq. (5).

$$E_{c,EM}(t, t_0) = \frac{E_c}{1 + \phi(t, t_0)} \quad (4)$$

$$E_{c,MS}(t, t_s) = \frac{E_c}{1 + 0.5\phi(t, t_s)} \quad (5)$$

where E_c is the elastic modulus of the concrete

$\phi(t, t_0)$ is the creep coefficient

t is the loading time

t_0 is the final time

t_s is the age of concrete at the beginning of shrinkage

According to Gilbert (1988), the creep coefficient changes with time and the values of the creep coefficient calculated are shown in Fig. 6. By using Eq. (6) below, the value of creep coefficient reduces the elastic modulus of concrete. The relationship of the elastic modulus of concrete with respect to time is illustrated in Fig. 7, which highlights that the elastic modulus of concrete is reduced with respect to time. It reduces significantly up to day 400, and after that the reduction value is less insignificant.

$$E'_c = E_c / (1 + \psi \phi) \quad (6)$$

where ϕ is the creep coefficient and ψ is an aging coefficient where the most appropriate value of 0.5 is used in the German design code, DIN 1045-1 (2001) to allow for time dependent induced stress.

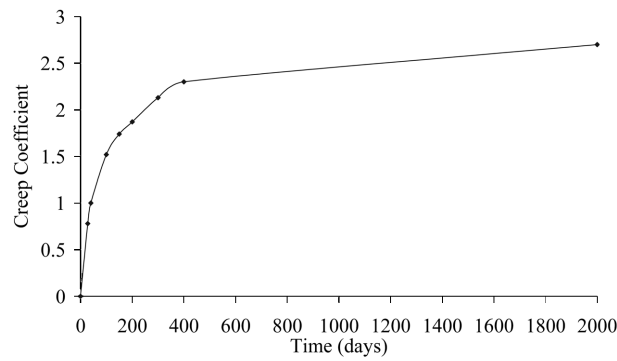


Fig. 6 Creep coefficient of concrete with respect to time, Gilbert (1988)

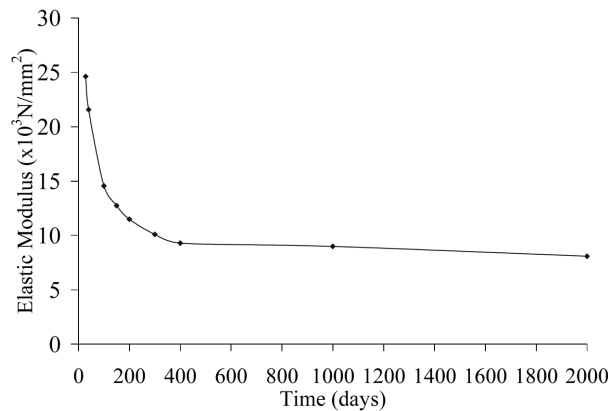


Fig. 7 Elastic modulus of concrete with respect to time, Gilbert (1988)

Bearing in mind that both equations suggested by Dezi, *et al.* (1998) and Gilbert (1988) are similar. Therefore authors proposed to apply the simplified algebraic method for the ABAQUS analysis herein.

3. Description of push test specimens

Experimental investigations undertaken by Lam and El-Lobody (2005) for solid slabs were used and compared with the finite element analysis when creep is taken into consideration. In order to compare the results of solid slabs used for calibration with W-DEK profiled steel sheeting slabs, the dimensions of the concrete slab, structural steel beams, steel reinforcement and shear connectors were held constant. In this paper authors only considered when shear connectors were positioned in the middle of the profiled sheeting. Mirza and Uy (2007) found that the strength of the shear connectors increased by 11% when they are placed in the strong side. Conversely when the shear connectors were positioned in the weak side, the strength of the shear connectors showed a reduction of 12.5%. All experiments were based on Eurocode 4, British Standards Institute (2004) which specifies a push test specimen that consists of a steel beam connected to two concrete slabs either solid slab or profiled slabs through shear connectors. However, some compromise has been made due to time limits, equipment and budget restrictions. The modified push tests shown in Figs. 8 and 9 involve slab dimensions of 619 mm \times 469 mm

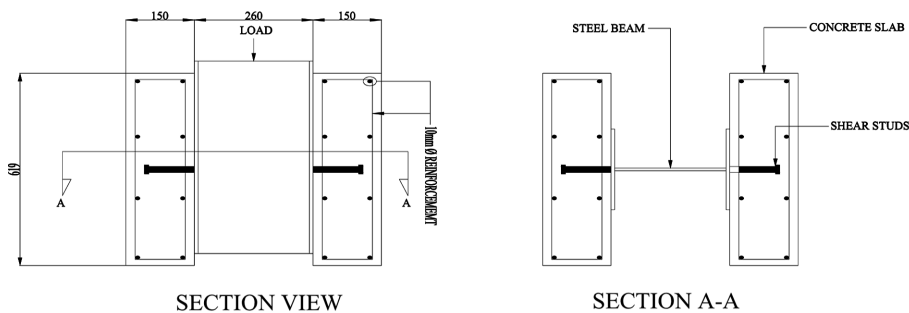


Fig. 8 Push test detail specimens for solid slab

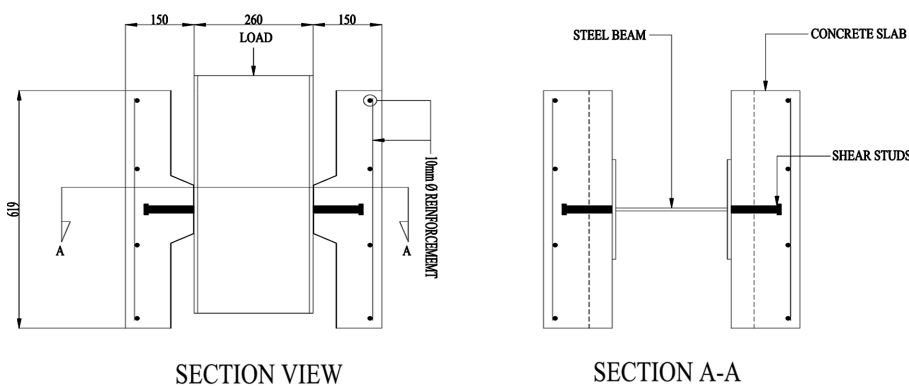


Fig. 9 Push test detail specimens for profiled slab

× 150 mm. In order to provide identical lateral and longitudinal reinforcement strength, 4 bars of 10 mm diameter reinforcement in each direction were used. The steel beam used was a 254 × 254 UC 73. Both the concrete slab and structural steel beam were attached to each other by 19 mm diameter shear connectors of 100 mm height.

4. Finite element model

4.1 General

The finite element program ABAQUS was used to simulate the behaviour of the shear connection in the composite beams when time effects are considered. Important components affecting the behaviour of shear connection are the concrete slab, steel beam, profiled steel sheeting, reinforcing bars and shear connectors. These components must be accurately defined to obtain an accurate result from the finite element analysis. A three dimensional finite element model has been developed to simulate the geometric and material nonlinear behaviour of a composite beam. The accuracy of the analysis depends greatly on the constitutive laws used to define the mechanical behaviour.

4.1.1 Concrete

The constitutive model for concrete by Carreira and Chu (1985) was used, where the linear elastic stress in compression is assumed up to a stress of $0.4f'_c$. Beyond this point, nonlinear response is observed and the stress-strain can be expressed as in Eq. (7).

$$\sigma_c = \frac{f'_c \gamma (\varepsilon_c / \varepsilon'_c)}{\gamma - 1 + (\varepsilon_c / \varepsilon'_c)^\gamma} \quad (7)$$

where and $\gamma = \left| \frac{f'_c}{32.4} \right|^3 + 1.55$ and $\varepsilon'_c = 0.002$

For concrete in tension, the tensile stress is assumed to increase linearly with tensile strain until the concrete cracks. After the concrete cracks, the tensile stresses decrease linearly to zero. The value of strain at zero stress is usually taken as 10 times the strain at failure which is illustrated in Fig. 10.

In this paper, a concrete damaged plasticity model was incorporated in the ABAQUS. According to Karlsson and Sonrensen (2006), the analysis concrete damaged plasticity model uses an isotropic damaged elasticity in combination with isotropic tensile and compressive plasticity, to better represent the inelastic behaviour of concrete. The concrete damaged plasticity in ABAQUS is used to define a yield function, flow potential, and viscosity parameters. Therefore, the model is suitable for the long-term analysis where viscosity parameters were used. Lubliner, *et al.* (1989) proposed that the concrete model uses a yield function with the modifications suggested by Lee and Fenves (1998) to consider different progression of strength characteristics under tension and compression. The progression of the yield surface is defined by hardening variables, known as equivalent tensile and compressive plastic strains. The equivalent tensile and compressive plastic strains are automatically calculated by ABAQUS after the definition of elastic material behaviour.

The plasticity based isotropic damage model proposed by Lee and Fenves (1998) is a model which is

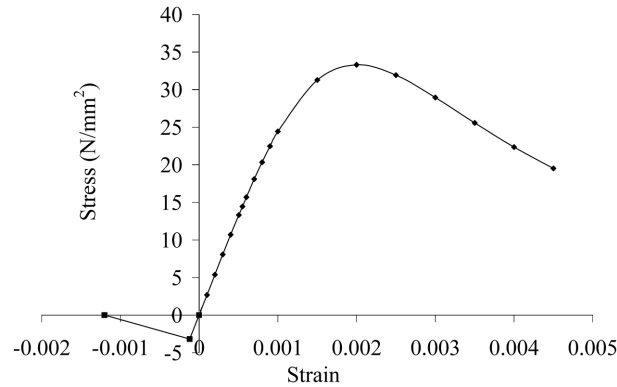


Fig. 10 Stress-strain relationship for concrete with respect to time, Carreira and Chu (1985)

specifically concerns the stress triaxiality dependent plastic hardening. The principal characteristic of the model include the damage evolution is not only connected to the increase in plastic strain, but also influenced explicitly by the elastic strain, the damage evolution is coupled with an increase in plastic strain and the stress triaxiality dependent plastic damage loading condition is defined in this model. The generalized Drucker Prager criterion for plastic loading, together with its plastic potential for the non-associated plastic flow rule, is referred to by the model herein.

4.1.2 Shear connectors, structural steel beam, profiled steel sheeting and steel reinforcing

The structural steel beam, profiled steel sheeting and steel reinforcing were each modelled in a piecewise linear fashion as an elastic-plastic material with strain hardening. The shear connectors were also modelled in a similar fashion as the structural steel beam, profiled steel sheeting and steel reinforcing but without the inclusion of strain hardening. The model developed by Loh, *et al.* (2003) shown in Fig. 11 and Table 1 indicated the different values of stress and strain for different materials.

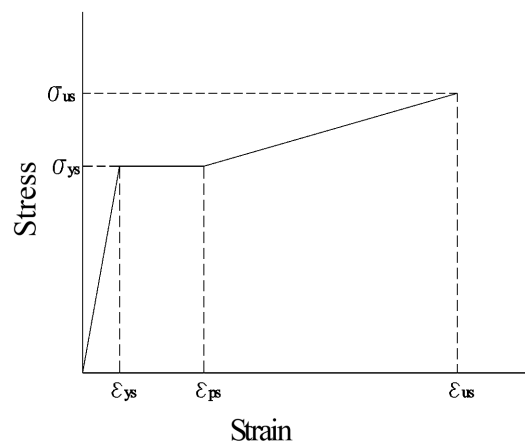


Fig. 11 Stress-strain relationship for structural steel beam, shear connectors, profiled steel sheeting and steel reinforcing (Loh, *et al.* 2003)

Table 1 Stress-strain value for structural steel beam, shear connectors, profiled steel sheeting and steel reinforcing.

Element	σ_{us}	ε_{ps}	ε_{us}
Steel beam	$1.28\sigma_{ys}$	$10\varepsilon_{ys}$	$30\varepsilon_{ys}$
Steel reinforcing	$1.28\sigma_{ys}$	$9\varepsilon_{ys}$	$40\varepsilon_{ys}$
Profiled sheeting	-	$20\varepsilon_{ys}$	-
Shear connectors	-	$25\varepsilon_{ys}$	-

4.2 Finite element mesh, boundary condition and load application

Boundary conditions that represent structural supports specify values of displacement and rotation variable at appropriate nodes. To facilitate a more economical solution, finite element meshes may also use symmetry where this can be implemented with a symmetrical boundary condition. Figs. 12 and 13 represents a quarter model of the push test conducted by Lam and El-Lobody (2005). Three dimensional solid elements were used to model a quarter of the push test specimens. Figs. 12 and 13 show a three

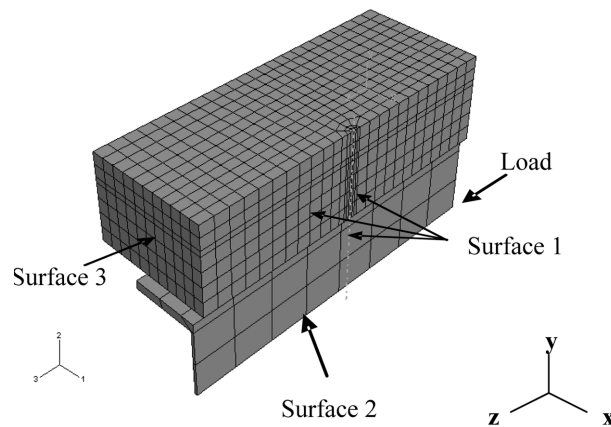


Fig. 12 Finite element model of push test specimen for solid slab

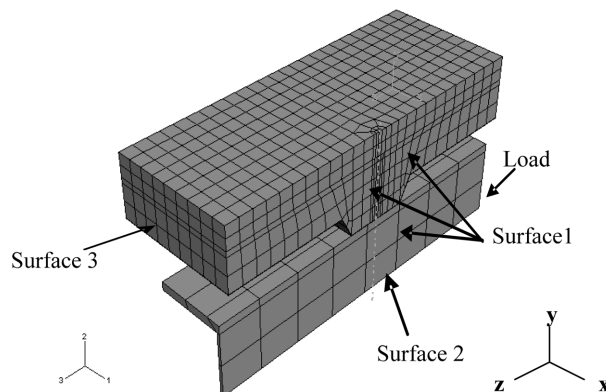


Fig. 13 Finite element model of push test specimen for profiled slab

dimensional eight node element (C3D8R) for both the concrete slab and structural steel beam, a three dimensional thirty node quadratic brick element (C3D20R) for the shear connector, a four node doubly curved thin shell element (S4R) for the profiled steel sheeting and a two node linear three dimensional truss element (T3D2) for the steel reinforcing. For the boundary conditions, surfaces 1, 2 and 3 were restricted to move in the x , y and z directions respectively. For the load application, a static concentrated load was applied to the centre of the web using the modified RIKS method. The modified RIKS method was employed to the load in order for the load to be obtained through a series of iterations for each increment for a non-linear structure. The RIKS method was used for the nonlinear analysis to ensure that any unloading was captured. Furthermore, this method was used to predict unstable and nonlinear collapse conditions of a structure. The load magnitude was used as an additional unknown and solved simultaneously for the loads and displacements. The model was also controlled by the slip of the shear connectors. The maximum slip that authors allowed is 14 mm and 10 mm for the solid and profiled slab respectively.

It should be borne in mind that the headed stud shear connector elements were bonded to the structural steel beam using tied contact interfaces. With this approach, each of the nodes on the headed stud shear connectors has the same displacement as the point adjacent to the surface of the structural steel beam. This allows for the modelling of normal and shear stresses along the entire structural steel beam and headed stud shear connectors interface. In ABAQUS, an appropriate allowance is incorporated in the finite element model to cover the effects of imperfections which include residual stresses.

5. Finite element analysis and discussions

In order to determine the effects of creep and shrinkage on composite steel-concrete beams, the push tests were analysed using ABAQUS to verify the shear capacity of the headed stud shear connectors. Fig. 14 showed that the finite element model prediction at 28 days are similar to the experimental results obtained by Lam and El-Lobody (2005). At 28 days, there is no consideration of time dependent behaviour to the concrete, the ultimate shear strength of the push test showed that the failure load was 105.4 kN, whilst, the finite element model resulted in a load of 102.6 kN. The discrepancy between experiment and finite element model was 2.6%. Therefore, the finite element model can be considered

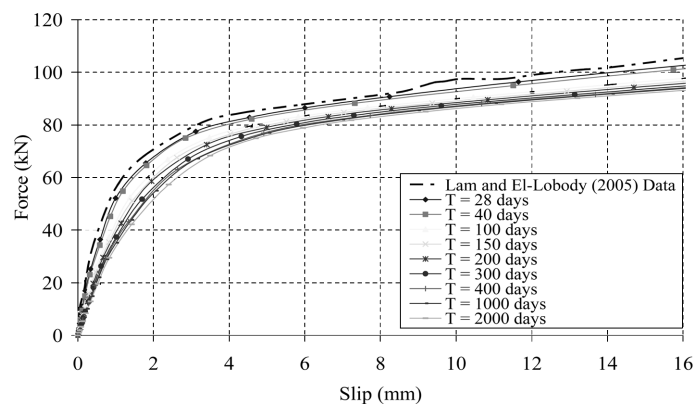


Fig. 14 Load versus slip relationship with respect to time for solid slab

to be reasonable in its estimation.

Ten finite element models were analysed for each solid and profiled slab shown in Table 2. Based on the finite element analyses, the variable parameters are time where the concrete behaviour changes when the creep and shrinkage is taken into consideration. It should be borne in mind that, for the purposes of comparison of the ultimate shear capacity for headed stud shear connectors in this study, the authors utilise the slip control function in ABAQUS. The author impedes the analyses at 16 mm for solid slabs in order to compare with the existing experimental study and 6 mm for profiled slabs.

Figs. 14 and 15 generally show that the shear capacity for solid slabs is higher than profiled slabs. It is

Table 2 Push test specimens parameters

Group	Push test specimens	Slab dimension (mm)	Steel beam	Shear stud dimension (mm)	Profiled steel sheeting thickness (mm)	Time (days)
G1	SPT1	619 × 469 × 150	254 × 254 UC73	19 × 100	0	0
	SPT2					28
	SPT3					40
	SPT4					100
	SPT5					150
	SPT6					200
	SPT7					300
	SPT8					400
	SPT9					1000
	SPT10					2000
G2	PPT1	619 × 469 × 150	254 × 254 UC73	19 × 100	10	0
	PPT2					28
	PPT3					40
	PPT4					100
	PPT5					150
	PPT6					200
	PPT7					300
	PPT8					400
	PPT9					1000
	PPT10					2000

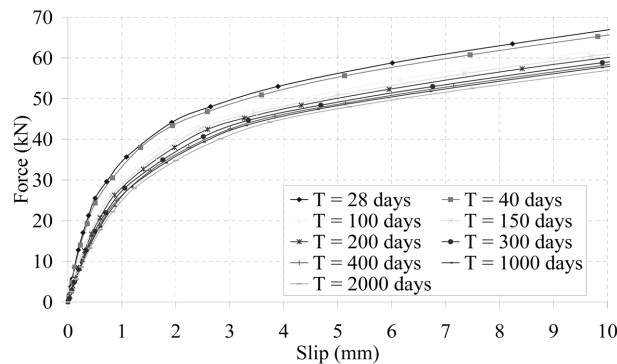


Fig. 15 Load versus slip relationship with respect to time for profiled slab

observed that both slabs behaved in a similar manner. The strength of the composite structure was reduced according to time when creep and shrinkage are taken into account. At the same time, creep and shrinkage also reduced the stiffness of the structure. Even though creep and shrinkage reduced the capacity of both the slabs, the solid slab had a greater slip and strength capacity when compared with the profiled slab.

The solid slab illustrated that the dominant failure mode was stud fracture where the shear connectors sheared off near the weld collar as shown in Fig. 16. The failure mode of the shear connector fracture is similar to that observed by Yam (1981) and Lam and El-Lobody (2005). The shear connectors experienced

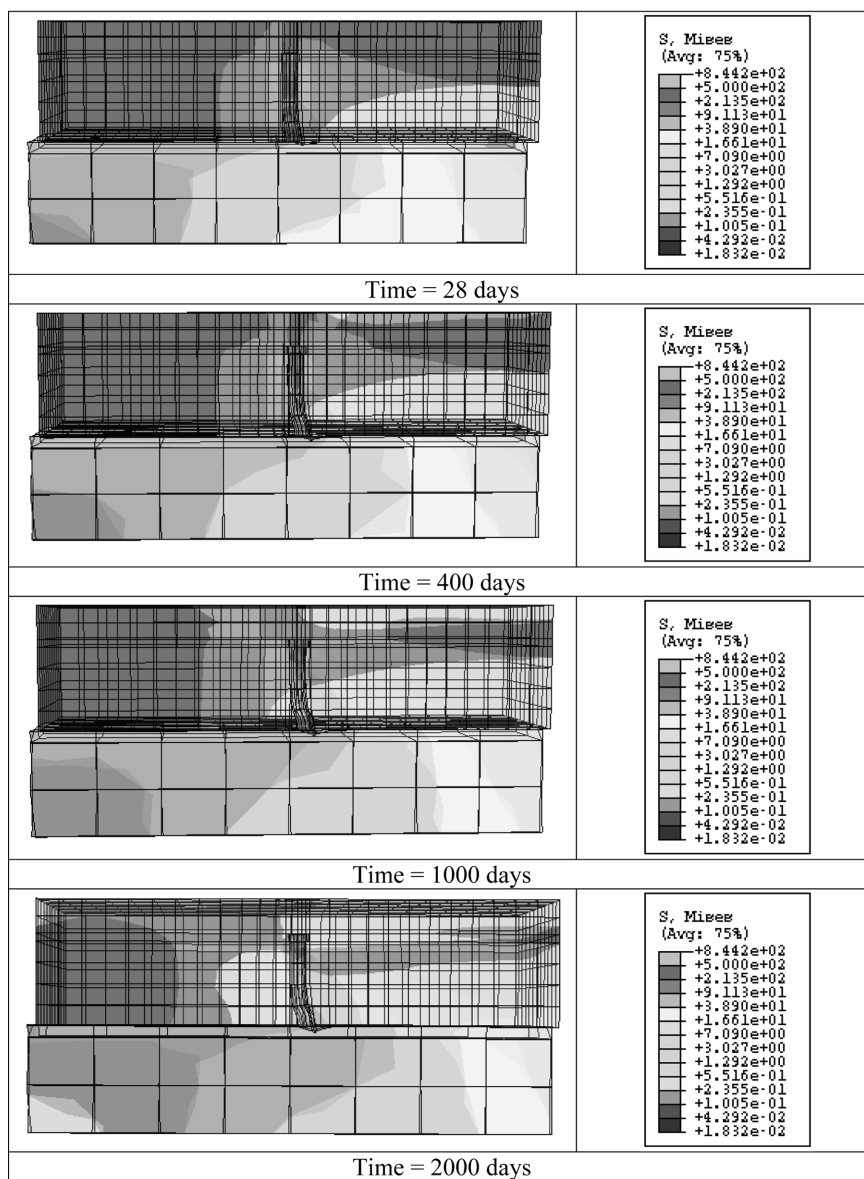


Fig. 16 Stress contours for push tests for solid slab

significant deformation around their base with time. The profiled slab showed signs of first cracking occurring in the middle of the slab along the trough of the profiled sheeting which was caused by concrete failure as shown in Fig. 17. Even though Kim, *et al.* (1999) stated that the inclusion of profiled steel sheeting resulted in less concrete cracking due to its contribution to the tensile strength but authors still noted that the failure mode was caused by concrete failure where the concrete cracked before the shear connectors fractured near the weld collar. The observed failure mode is similar to that mentioned by El-Lobody and Young (2006).

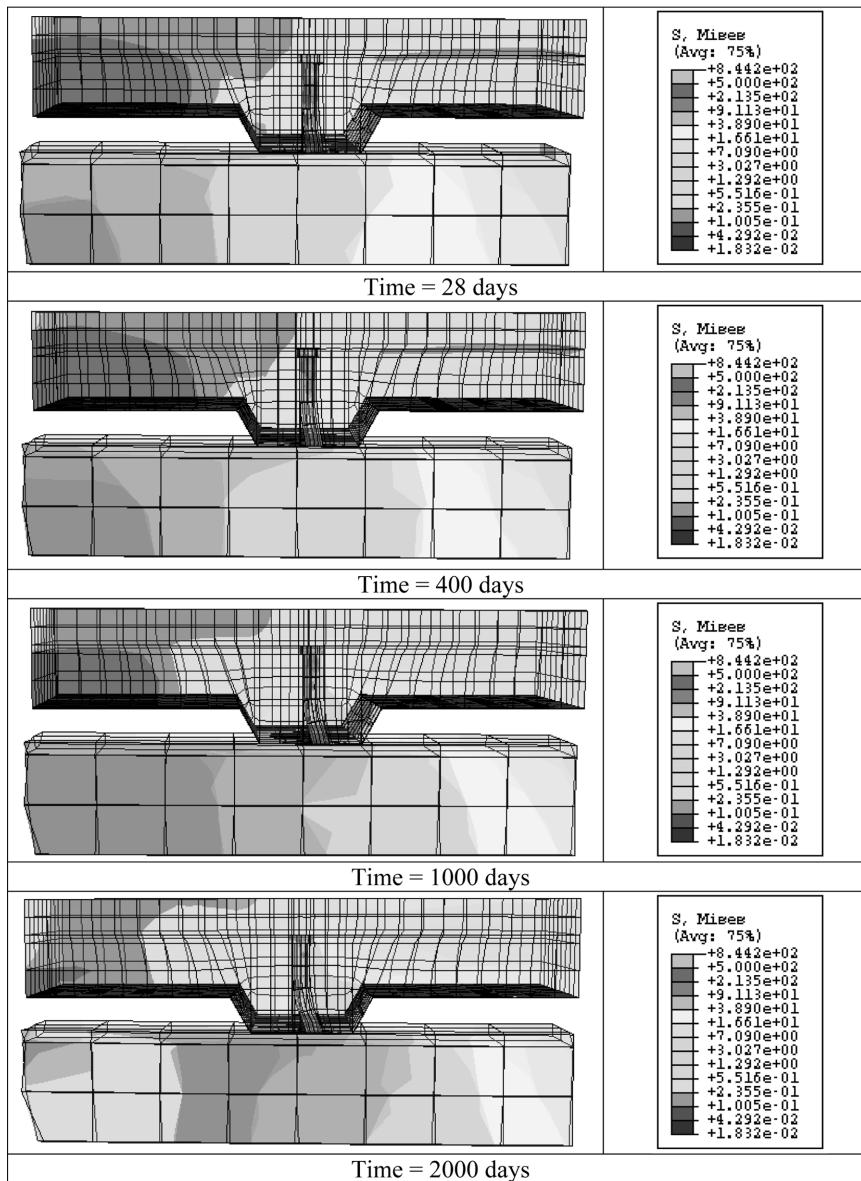


Fig. 17 Stress contours for push tests for profiled slab

Based on the results of push test finite element analyses, a series of numerical analyses has been carried out which established the progression of shear force resistance when creep and shrinkage is incorporated. The shear forces were measured according to an ultimate slip of standard rate of 4 mm. The shear force ratio, $P(t)/P_{(28)}$ related to different time periods of the push tests are plotted in Fig. 18. The solid slab showed a reduction of 12% of shear force resistance while the profiled slab showed a 16% reduction. Both slabs illustrated that the shear force reduced significantly up to 400 days, after that the reduction value was not significant. Creep is dependent on stress and affected area. Fig. 19 shows the stress distribution for both solid and profiled slabs. In Fig. 19(a), when Region A is compared to

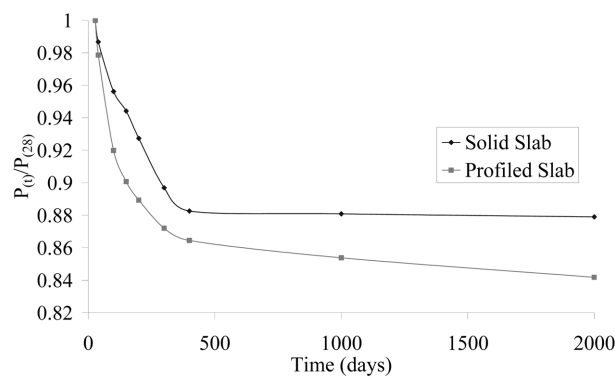


Fig. 18 Shear resistance of shear connectors with respect to time for ultimate slip rate = 4 mm

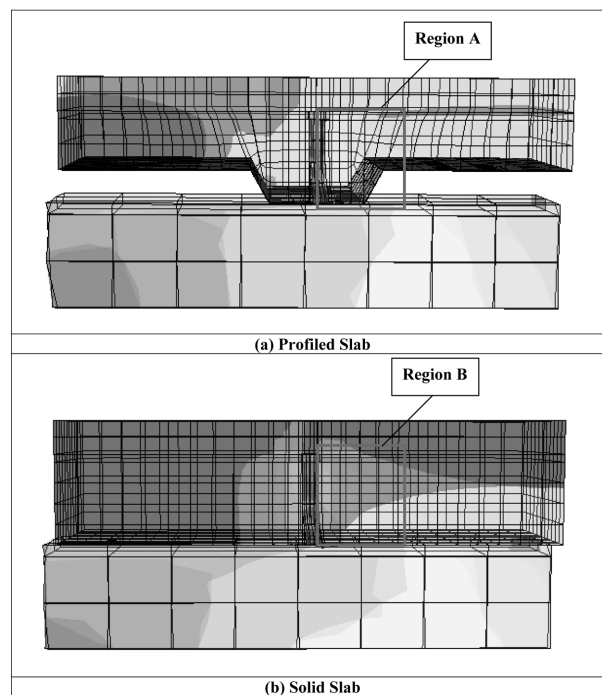


Fig. 19 Push test showing stress distribution

Region B, the affected area is smaller. When the affected area is smaller, the stress will tend to accumulate in Region A more so than Region B. In time, Region A develop a higher stress than Region B, and with the combination of less concrete area, the profiled slab shows a higher reduction in shear force resistance than the solid slab.

From Fig. 20, slip for both slabs behaved correspondingly and it is observed that the slip increases significantly in the first 400 days, and then the increase becomes insignificant. Therefore, it can be assumed that time dependent slip can be ignored after 400 days. The slip capacity for solid slabs was higher than profiled slab.

6. Parametric studies

An extensive parametric study consisting thirty two series of tests was conducted using the finite element model to look at the effect of creep and shrinkage analysis on the behaviour of headed stud shear connectors for both solid and profiled slabs. The verified finite element model was used to conduct a parametric study aiming to investigate the effect of several parameters, such as height and thickness of connector and concrete compressive strength on the headed stud shear resistance capacity. Constants were the number of stud connectors per slab, steel reinforcement, concrete slab dimensions, structural steel beam and profiled steel sheeting. Each series consisted of ten tests where the push tests were subjected to variable time which ranged from 28 to 2000 days. Table 3 shows the headed stud shear connectors used were 13, 16, 19 and 22 mm with various concrete strengths of 25, 30, 35 and 40 N/mm².

Table 4 shows the obtained ultimate shear capacity of headed stud shear connectors with varying diameters and concrete strength from the finite element model. The results show that the ultimate shear capacity for all the headed shear stud connectors increased with the increase in concrete strength. Table 4 also demonstrates that for all the headed stud shear connectors, the failure mode is governed by concrete failure with the lower concrete strength, whilst with the higher concrete strength, the failure mode is dominated by stud yielding failure. The purpose of these tests is described below.

6.1. Effects of headed stud shear connectors

The first parameter evaluated was the effect of height and thickness of the headed stud shear

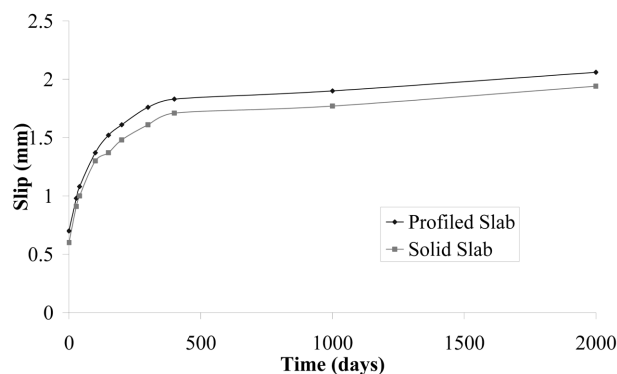


Fig. 20 Slip behaviour of shear connectors with respect to time

Table 3 Parametric study for push test specimens

Group	Push test specimens	Slab dimension (mm)	Concrete strength (N/mm ²)	Shear stud dimension (mm)	Profiled steel sheeting thickness (mm)
PG1	T1-T10	619 × 469 × 150	25	13 × 65	0
PG2	T1-T10	619 × 469 × 150	25	16 × 75	0
PG3	T1-T10	619 × 469 × 150	25	19 × 100	0
PG4	T1-T10	619 × 469 × 150	25	22 × 100	0
PG5	T1-T10	619 × 469 × 150	30	13 × 65	0
PG6	T1-T10	619 × 469 × 150	30	16 × 75	0
PG7	T1-T10	619 × 469 × 150	30	19 × 100	0
PG8	T1-T10	619 × 469 × 150	30	22 × 100	0
PG9	T1-T10	619 × 469 × 150	35	13 × 65	0
PG10	T1-T10	619 × 469 × 150	35	16 × 75	0
PG11	T1-T10	619 × 469 × 150	35	19 × 100	0
PG12	T1-T10	619 × 469 × 150	35	22 × 100	0
PG13	T1-T10	619 × 469 × 150	40	13 × 65	0
PG14	T1-T10	619 × 469 × 150	40	16 × 75	0
PG15	T1-T10	619 × 469 × 150	40	19 × 100	0
PG16	T1-T10	619 × 469 × 150	40	22 × 100	0
PG17	T1-T10	619 × 469 × 150	25	13 × 65	10
PG18	T1-T10	619 × 469 × 150	25	16 × 75	10
PG19	T1-T10	619 × 469 × 150	25	19 × 100	10
PG20	T1-T10	619 × 469 × 150	25	22 × 100	10
PG21	T1-T10	619 × 469 × 150	30	13 × 65	10
PG22	T1-T10	619 × 469 × 150	30	16 × 75	10
PG23	T1-T10	619 × 469 × 150	30	19 × 100	10
PG24	T1-T10	619 × 469 × 150	30	22 × 100	10
PG25	T1-T10	619 × 469 × 150	35	13 × 65	10
PG26	T1-T10	619 × 469 × 150	35	16 × 75	10
PG27	T1-T10	619 × 469 × 150	35	19 × 100	10
PG28	T1-T10	619 × 469 × 150	35	22 × 100	10
PG29	T1-T10	619 × 469 × 150	40	13 × 65	10
PG30	T1-T10	619 × 469 × 150	40	16 × 75	10
PG31	T1-T10	619 × 469 × 150	40	19 × 100	10
PG32	T1-T10	619 × 469 × 150	40	22 × 100	10

*T1 denotes 0 day, T2 denotes 28 days, T3 denotes 40 days, T4 denotes 100 days, T5 denotes 150 days, T6 denotes 200 days, T7 denotes 300 days, T8 denotes 400 days, T9 denotes 1000 days and T10 denotes 2000 days

connectors on the composite steel-concrete beams. Conventionally, push-out tests have used 19 × 100 headed stud shear connectors. Thirty tests were performed to verify that the height and thickness of headed stud shear connectors would cause changes in the ultimate capacity of composite steel-concrete beams. The desired mode of failure for composite steel-concrete structures was stud shearing failure. From the parametric studies, the headed stud shear connectors with 13 × 65 mm and 16 × 75 mm show a lower stud capacity than 19 × 100 mm and 22 × 100 mm studs. When 19 and 22 mm diameter are used, the resistance against concrete splitting is provided by the capacity of the headed stud shear connectors. The push test specimens with smaller stud diameter reduced the shear capacity than those with bigger stud diameter. Push test specimens with 19 and 22 mm diameter studs only failed when the

Table 4 Results of parametric study for push test specimens

Ultimate Shear Capacity for Headed Studs Shear Connector for Solid Slab (kN)																
Day	25 N/mm ²				30 N/mm ²				35 N/mm ²				40 N/mm ²			
	13 × 65	16 × 75	19 × 100	22 × 100	13 × 65	16 × 75	19 × 100	22 × 100	13 × 65	16 × 75	19 × 100	22 × 100	13 × 65	16 × 75	19 × 100	22 × 100
28	40.0	58.9	85.4	99.7	45.6	65.5	95.6	115.6	48.9	72.4	101.7	125.4	53.2	78.3	107.8	138.6
40	39.5	58.1	84.3	98.4	45.0	64.6	94.3	114.1	48.3	71.4	100.4	123.7	52.5	77.3	106.4	136.8
100	38.2	56.3	81.7	95.3	43.6	62.6	91.4	110.5	46.8	69.2	97.2	119.9	50.9	74.9	103.1	132.5
150	37.8	55.6	80.6	94.1	43.1	61.8	90.3	109.1	46.2	68.4	96.0	118.4	50.2	73.9	101.8	130.9
200	37.1	54.6	79.2	92.5	42.3	60.7	88.7	107.2	45.3	67.1	94.3	116.3	49.3	72.6	100.0	128.5
300	35.9	52.8	76.6	89.4	40.9	58.7	85.7	103.7	43.9	64.9	91.2	112.5	47.7	70.2	96.7	124.3
400	35.3	52.0	75.4	88.0	40.2	57.8	84.4	102.0	43.2	63.9	89.8	110.7	47.0	69.1	95.1	122.3
1000	35.2	51.9	75.2	87.8	40.2	57.7	84.2	101.8	43.1	63.8	89.6	110.5	46.9	69.0	95.0	122.1
2000	35.2	51.8	75.1	87.6	40.1	57.6	84.0	101.6	43.0	63.6	89.4	110.2	46.8	68.8	94.8	121.8

Ultimate Shear Capacity for Headed Studs Shear Connector for Profiled Slab (kN)																
Day	25 N/mm ²				30 N/mm ²				35 N/mm ²				40 N/mm ²			
	13 × 65	16 × 75	19 × 100	22 × 100	13 × 65	16 × 75	19 × 100	22 × 100	13 × 65	16 × 75	19 × 100	22 × 100	13 × 65	16 × 75	19 × 100	22 × 100
28	21.1	31.1	45.1	52.6	25.1	36.1	52.9	64.5	28.6	42.4	59.5	73.4	31.9	46.9	64.6	83.1
40	20.6	30.4	44.1	51.5	24.5	35.3	51.8	63.1	28.0	41.4	58.2	71.8	31.2	45.9	63.2	81.3
100	19.4	28.6	41.5	48.4	23.1	33.2	48.7	59.3	26.3	39.0	54.7	67.5	29.3	43.1	59.4	76.4
150	19.0	28.0	40.6	47.4	22.6	32.5	47.6	58.1	25.8	38.1	53.6	66.1	28.7	42.2	58.2	74.8
200	18.8	27.6	40.1	46.8	22.3	32.1	47.0	57.4	25.4	37.7	52.9	65.3	28.4	41.7	57.4	73.9
300	18.4	27.1	39.3	45.9	21.9	31.5	46.1	56.2	24.9	36.9	51.9	64.0	27.8	40.9	56.3	72.4
400	18.2	26.9	39.0	45.5	21.7	31.2	45.7	55.8	24.7	36.6	51.4	63.5	27.6	40.5	55.8	71.8
1000	18.0	26.5	38.5	44.9	21.4	30.8	45.2	55.1	24.4	36.2	50.8	62.7	27.2	40.0	55.1	70.9
2000	17.8	26.1	38.0	44.3	21.1	30.4	44.5	54.3	24.1	35.7	50.1	61.8	26.8	39.5	54.4	69.9

ultimate strength of the headed stud was reached. This effect is particularly important when a partial shear connection design is adopted when the ductility of the shear connectors becomes an important issue.

6.2 Effects of concrete compressive strength

The second parameter investigated was the effect on stud strength of the concrete compressive strength. These tests were used to determine if the stud strength was reduced by changing the concrete compressive strength. The stud strength increased when higher concrete compressive strength was used. Thus one could conclude that using a higher concrete compressive strength in composite steel-concrete specimens automatically increases the stud strength. Higher concrete compressive strength will have lower concrete splitting. Therefore, for a higher concrete compressive strength, when the concrete splitting occurs, the tensile strength developed by the headed stud shear connectors is much higher, and the shear resistance of the stud will rise. From the parametric studies, the failure modes changes from concrete failure at the lower concrete compressive strength to stud shearing failure at the higher concrete compressive strength. Lower concrete compressive strength showed that the failure of push-out specimens tested occurred in concrete slab and initiated by longitudinal splitting of the slab which is similar as mentioned in Liu (2006). When higher concrete compressive strength was used, the stud will achieve the maximum stress before the concrete reaches its tensile stress. This is the reason why the headed stud shear connectors reached their maximum capacity before concrete failure.

7. Conclusions

This paper discusses three key issues in the finite element model for push tests. In order to prove that an accurate finite element model has been developed to investigate the behaviour of the shear connection in composite steel-concrete beams for both solid and profiled slabs when creep and shrinkage is taken into account, the finite element models were initially compared with existing push test experimental studies. From the series of finite element analyses, when creep and shrinkage are considered, the reduction in stiffness, ultimate shear capacity and slip capacity for both the solid and profiled slabs was observed. From the finite element analyses, the solid slab demonstrated that the failure mode is dominated by shear yielding failure, whilst failure in the profiled slabs can be attributed to concrete failure.

There are three differences between the profiled sheeting and solid slabs. For the solid slab, the failure mode is shear connector failure, whilst failure in the profiled slabs can be attributed to concrete failure. It also can be observed that the solid slab generally had a higher ultimate shear capacity and slip capacity when compared with the profiled steel sheeting slab. Lastly, it is concluded that creep caused by the slip of the shear connectors was noticeable in the first 400 days, and the Young's Modulus of the concrete is reduced accordingly, leading to significant reduction in the shear resistance of the headed stud shear connection. After 400 days, creep did not have a major influence on the mechanical behaviour of composite steel and concrete structures.

The parametric studies shown in Section 6 is able to simulate the overall behaviour of headed stud shear connectors in push testing when creep and shrinkage are included in the concrete slab. Most of the push tests analysed by the author contained either solid slab or profiled slab with WDEK profile of 10 mm thick. Strictly speaking, the result revealed herein is only relevant for such cases mentioned above only. Graphs based on the numerical analyses were produced and are suitable for practising engineers to estimate the shear capacity of the headed stud shear connectors for design purposes. Figs. 21 to 24

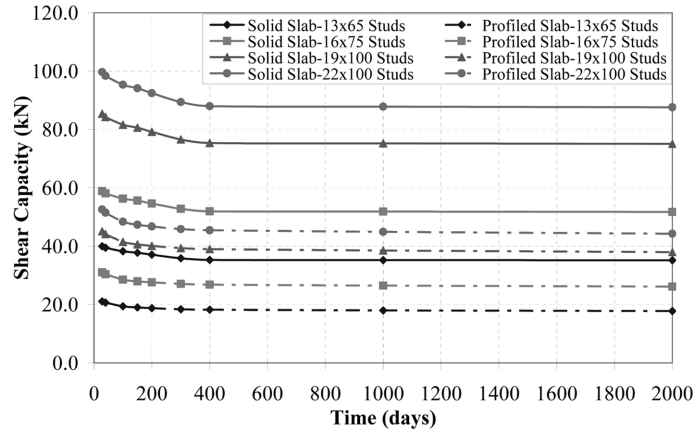


Fig. 21 Shear capacity with respect to time for 25 N/mm² concrete strength

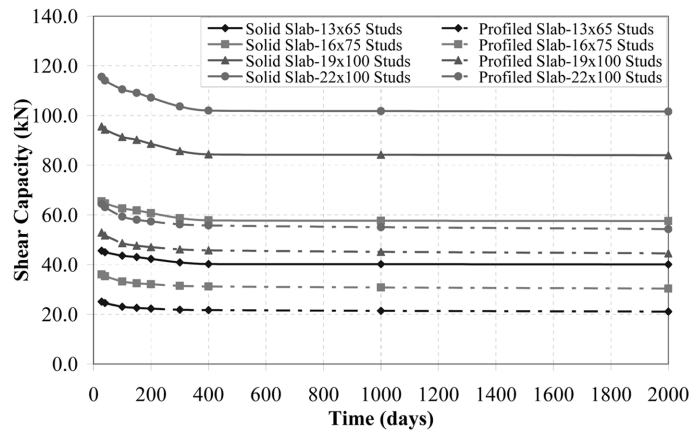


Fig. 22 Shear capacity with respect to time for 30 N/mm² concrete strength

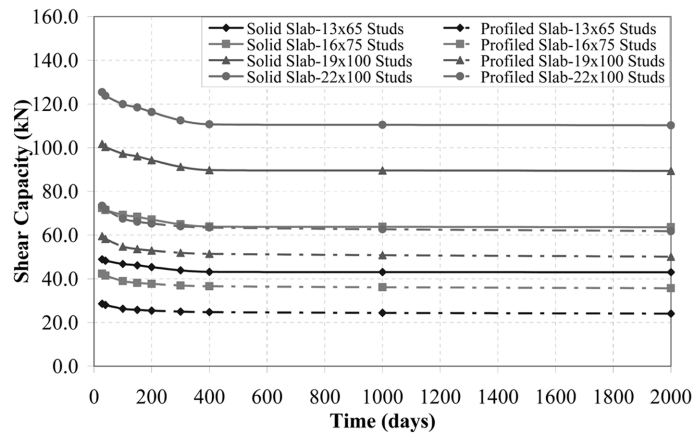


Fig. 23 Shear capacity with respect to time for 35 N/mm² concrete strength

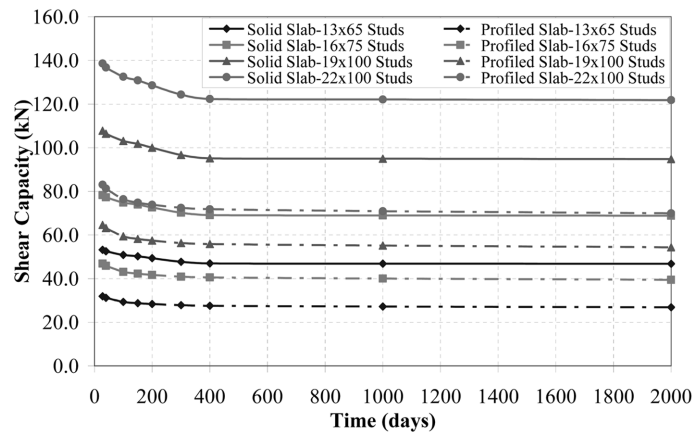


Fig. 24 Shear capacity with respect to time for 40 N/mm² concrete strength

illustrate the ultimate shear capacity according to time for solid and profiled slabs with concrete strengths of 25, 30, 35, and 40 N/mm², respectively.

Composite steel-concrete beams with creep taken into account show a reduction in stiffness and slip capacity. Experimental studies considering composite steel-concrete beams when creep is taken into account and with the inclusion of steel fibres to look at the stiffness and ductility will be subjected to future research in this project compared with finite element analysis.

Acknowledgements

The authors would like to thank the Australian Research Council Linkage Program and BlueScope Lysaght in Sydney for providing funding to this project and The University of Western Sydney for their support to the authors work described herein.

References

- Bradford, M.A. (1991), "Deflection of composite steel-concrete beams subjected to creep and shrinkage", *ACI Struct. J.*, **88**(5), 610-614.
- Bradford, M.A. and Gilbert, R.I. (1989), "Nonlinear behaviour of composite beams at service loads", *J. Struct. Eng.*, **67**(14), 263-268.
- Bradford, M.A. and Gilbert, R.I. (1992), "Composite beams with partial interaction under sustained loads", *J. Struct. Eng.*, **118**(7), 1871-1883.
- British Standards Institute (2004), *Design of composite steel and concrete structures, Part 1.1 General rules and rules for buildings*, British Standard Institute, London.
- Carreira, D. and Chu, K. (1985), "Stress-strain relationship for plain concrete in compression", *ACI Struct. J.*, **82**(11), 797-804.
- CEB-FIP (1990), *Comité Euro-International Du Béton*, London. London.
- Dezi, L., Leoni, G. and Tarantino, A.M. (1995), "Time dependent analysis of prestressed composite beams", *J. Struct. Eng.*, **121**(4), 612-633.
- Dezi, L., Leoni, G. and Tarantino, A.M. (1998), "Creep and shrinkage analysis of composite beams", *J. Struct.*

- Eng. Mater.*, **1**(2), 170-177.
- Dezi, L. and Tarantino, M. (1993), "Creep in composite continuous beams II: parametric study", *J. Struct. Eng. ASCE*, **119**, 2112-2133.
- di Prisco, M. and Mazars, J. (1996), "Crush-crack: A non-local damage model for concrete. Mechanical Cohesive-Friction Material", *Int. J. Numer. Anal. Met.*, **1**(4), 223-230.
- DIN 1045-1 (2001), *Plain concrete, reinforced and prestressed concrete structures - Part 1: Design and construction*.
- El-Lobody, E. and Young, B. (2006), "Performance of shear connection in composite beams with profiled steel sheeting", *J. Constr. Steel Res.*, **62**(7), 682-694.
- Ghali, A., Favre, R. and Elbadry, M. (2002), *Concrete structures - stresses and deformation*, New York 10001, Spon Press.
- Gilbert, R.I. (1988), *Time effects in concrete structures*, Amsterdam, The Netherlands, Elsevier Science Publishers.
- Gilbert, R.I. and Bradford, M.A. (1995), "Time-dependent behavior of continuous composite beams at service loads", *J. Struct. Eng. ASCE*, **121**(2), 319-327.
- Johnson, R.P. (1974), *Composite structures of steel and concrete*, London, England, Collins.
- Karlsson and Sonrensen (2006), *ABAQUS, Theory manual version 6.5*, Pawtucket, Rhode Island, Hibbit Publication.
- Kim, B., Wright, H.D., Cairns, R. and Bradford, M.A. (1999), "The numerical simulation of shear connection", *Proc. of the 16th Australasian Conf. on The Mechanics of Structures and Materials*, Sydney, NSW, Australia.
- Krajcinovic, H.B. and Fonseka, G.U. (1981), "The continuous damage theory of brittle materials II: Uniaxial and plane response modes", *J. Appl. Mech.*, **48**, 806-860.
- Kupfer, H.B., Hilsdorf, H.K. and Rusch, H. (1969), "Behaviour of concrete under biaxial stresses", *ACI Struct. J.*, **66**, 656-666.
- Kwak, H.G., Seo, Y.J. and Jung, C.M. (2000), "Effects of the slab casting sequences and the drying shrinkage of concrete slabs on the short-term and long-term behavior of composite steel box girder bridges. Part 2", *Eng. Struct.*, **23**, 1467-1480.
- Lam, D. and El-Lobody, E. (2005), "Behaviour of headed stud shear connectors in composite beam", *J. Struct. Eng. ASCE*, **131**(1), 96-107.
- Lee, J. and Fenves, G.L. (1998), "Plastic damage model for cyclic loading of concrete", *J. Eng. Mech.*, **124**(8), 892-900.
- Liu, Y.Q. (2006), *Experimental and analytical investigation of Naning steel-concrete composite bridge arch*, Bridge Engineering Department, Tongji University, Shanghai, China, 72.
- Loh, H.Y., Uy, B. and Bradford, M.A. (2003), "The effects of partial shear connection in the hogging moment region of composite beams Part II - analytical study", *J. Constr. Steel., Res.*, **60**, 921-962.
- Lubliner, J., Oliver, S. and O'Nate Oller, E. (1989), "A plastic-damage model for concrete", *J. Solids Struct.*, **25**, 200-329.
- Mazzotti, C. and Savoia, M. (2003), "Nonlinear creep damage model for concrete under uniaxial compression", *J. Eng. Mech.*, **129**(9), 1065-1075.
- Mazzotti, C., Savoia, M., Cadoni, E. and Pedretti, A. (2000), "Experimental investigation on the crack pattern evolution of concrete in compression using ESPI technique", *Proc. Int. Conf. on Trends in Optical Nondestructive Testing*, Lugano, Switzerland, K. Rastogi and D. Inaudi.
- Mirza, O. and Uy, B. (2007), "Effect of steel fibre reinforcement on the shear connection of composite steelconcrete beams", *J. Adv. Steel Constr.*, **5**(1), 72-95.
- Tarantino, A.M. and Dezi, L. (1992), "Creep effects in composite beams with flexible shear connectors", *J. Struct. Eng.*, **118**(8), 2063-2081.
- Yam, L.C.P. (1981), *Design of composite steel-concrete structures*, London, Surrey University Press.

Notation

E	Young's modulus
E_c	elastic modulus for the concrete
$E_{c,EM}$	modified elastic modulus for the effective method
$E_{c,MS}$	modified elastic modulus for the mean stress method
f_c, f'_c	characteristic compressive strength of concrete
P_t	ultimate load at time t
$P_{(28)}$	ultimate load at 28 days
t	time
t_r	time application of stress
t_s	age of concrete in days when shrinkage start
t_0	the time of load application
β_s	the coefficient to represent the development of shrinkage according to time
$\varepsilon^{el,d}$	the effective strain which is the sum of instantaneous strains
ε_c	concrete compressive strain
ε'_c	strain corresponding to f'_c
ε_{cr}	creep strain
ε_{sh}	shrinkage strain
ε_{ps}	strain value before strain hardening begins
$\varepsilon_{p,\theta}$	strain at the proportional limit
ε_{us}	ultimate yield strain of the steel structure
ε_{eff}^y	the fraction of viscous strain which is obtained from an age loading at a time
ε_{ys}	yield strain of the steel structure
γ	parameter used to define stress-strain curve for concrete
σ_c	concrete compressive stress
σ_t	tensile strength of concrete
σ_{us}	ultimate stress of the steel material
σ_{ys}	yield stress of the steel material
ψ	aging coefficient for concrete
χ	aging coefficient
ϕ	creep coefficient